

## Photoelectron Imaging of Helium Droplets

Darcy S. Peterka,<sup>1,2</sup> Albrecht Lindinger,<sup>2</sup> Lionel Poisson,<sup>1,2</sup> Musahid Ahmed,<sup>2</sup> and Daniel M. Neumark<sup>1,2</sup>

<sup>1</sup>*Department of Chemistry, University of California, Berkeley, California 94720, USA*

<sup>2</sup>*Chemical Sciences Division, Lawrence Berkeley National Laboratory, Berkeley, California 94720, USA*

(Received 27 November 2002; published 25 July 2003)

The photoionization and photoelectron spectroscopy of He nanodroplets ( $10^4$  atoms) has been studied by photoelectron imaging with photon energies from 22.5–24.5 eV. Total electron yield measurements reveal broad features, whose onset is  $\sim 1.5$  eV below the ionization potential of atomic He. The photoelectron spectra are dominated by very low energy electrons, with  $\langle E_k \rangle$  less than 0.6 meV. These results are attributed to the formation and autoionization of highly vibrationally excited  $\text{He}_n^*$  Rydberg states within the cluster, followed by strong final state interactions between the photoelectron and the droplet.

DOI: 10.1103/PhysRevLett.91.043401

PACS numbers: 36.40.-c, 33.20.Ni, 33.60.Cv, 33.80.Eh

Helium nanodroplets have been shown to be a novel spectroscopic medium, providing a “quantum matrix” in which one can probe the rotational, vibrational, and electronic spectroscopy of various dopants and see how they are affected by the interactions with the surrounding He atoms [1,2]. On the other hand, the spectroscopy of pure He droplets has presented quite a challenge. The optically allowed electronic transitions of He droplets lie well above the energy range accessible to laser spectroscopy, restricting experiments to synchrotron light sources. Thus far, fluorescence excitation spectra between 20–25 eV have been measured [3–5], as has the photoionization efficiency as a function of photon energy and droplet size [6]. These experiments raise the issue of the mechanism of ionization in pure He droplets, the competition between the mechanisms leading to ionization vs fluorescence, and the interaction of the photoelectron with the atoms in the droplet. In order to address these and other issues, we have performed the first photoelectron spectroscopy experiments on  $\text{He}_N$  droplets with  $N \sim 10^4$ . Our results show strong evidence for many-body effects and final state interactions between the photoelectron and the He atoms in the droplet.

The experiments were carried out on the Chemical Dynamics Beamline at the Advanced Light Source [7]. He droplets were ionized by tunable synchrotron radiation, and the photoelectron energy and angular distributions were determined by photoelectron imaging. The continuous He droplet beam was generated in a source based on designs used by the groups of Frochtenicht, Nauta, and Toennies [6,8,9]. The droplets were produced by expanding  $\sim 30$  bars of helium gas through a  $5 \mu\text{m}$  aperture on a source cooled with a closed cycle helium refrigerator operated with nozzle temperatures of 10–18 K. The nozzle assembly was shielded from thermal radiation by a liquid  $\text{N}_2$  cooled copper shroud that also served to precool the He gas.

The droplet beam then passed through a 1 mm skimmer and entered the ionization region within the main chamber. Vacuum ultraviolet (VUV) radiation from a

10 cm period undulator was dispersed by a 3 m normal incidence, off-plane Eagle monochromator, yielding more than  $10^{13}$  photons/s at 25 eV with a bandwidth of 15 meV. In the main chamber, the light crossed the helium droplet beam perpendicular to the axis of the electron detection system, comprising electron extraction optics, a 0.5 m flight tube, and a microchannel plate (MCP) detector coupled to a phosphor screen and charge-coupled device detector (Fig. 1). The polarization of the undulator beam was parallel to the plane of the electron detector. The electron optics were biased to achieve “velocity map” conditions [10], so that all electrons with the same momentum in the plane parallel to the detector were imaged to the same point, reducing spatial blurring. The electric field in the interaction region was  $\sim 120$  V/cm. A photomultiplier tube monitored the light from the phosphor screen, allowing for simultaneous total electron yield measurements. Electron kinetic energy ( $E_k$ ) and angular distributions were obtained from images using standard methods.

Figure 2 shows the total electron yield (TEY) following photoexcitation between 22.5 to 24.6 eV along with the location of He atomic  $np$  Rydberg states. The solid line is the spectrum taken with the cryostat on (12 K),

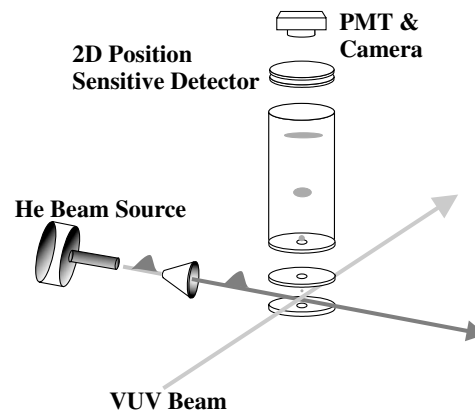


FIG. 1. Schematic of experimental apparatus (see text).

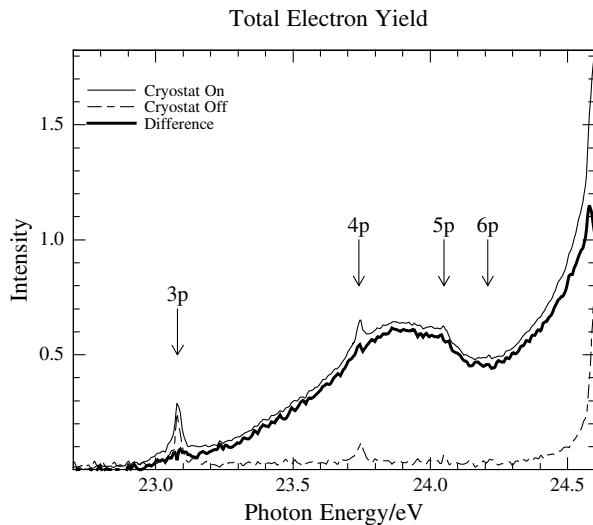


FIG. 2. Total electron yield spectra. Thin solid line: helium droplet beam (cryostat on,  $\sim 11$  K). Dashed line: atomic helium beam (cryostat off,  $> 40$  K). Bold solid line: difference spectrum. The atomic singlet  $np$  Rydberg states are also indicated.

which results in droplet formation with  $\langle N \rangle \sim 10^4$  atoms [11]. The dashed line is the spectrum taken with the cryostat off ( $> 40$  K), yielding a beam of He atoms. The difference spectrum is shown in bold. In the droplet and difference spectrum, the onset of photoelectrons occurs at about 23.0 eV. The TEY increases slowly, peaking near 23.85 eV, then dips slightly, forming a broadband. As the atomic He ionization threshold at 24.587 eV is approached, the electron yield increases rapidly. There are sharp features located at 23.08, 23.74, and 24.05 eV superimposed on the broad structure of the “cryostat on” spectrum, coinciding with He ( $np$ ) Rydberg states, and lining up perfectly with features in the electron yield spectrum produced with the cryostat off. In the difference spectrum, only the broad features remain. As atomic He cannot ionize at these energies, we attribute the sharp peaks in the TEY spectra to VUV fluorescence from He atoms that is detected by the MCP—an assignment supported by a series of retarding field measurements showing that while the large broad features disappear, the sharp features persist.

The onset of photoelectrons at 23.0 eV and the broad peak at 23.85 eV were also seen in the total ion yield measurements by Frochtenicht *et al.* [6], although the signal-to-noise ratio appears to be considerably better in our experiments. In the energy range where electrons are observed, the TEY spectrum is also similar to the fluorescence excitation spectrum of droplets in the  $10^4$  atom size range measured by Joppien *et al.* [3].

A representative photoelectron image and its corresponding  $E_k$  distribution are shown in Fig. 3. The photon energy was 23.8 eV, near the maximum of the broad peak in the total electron yield spectrum. The electron signal is concentrated at the center of the detector, with  $\sim 20\%$  of the total intensity filling 1% of the total area. In the  $E_k$

distribution, the electrons corresponding to the central spot have a maximum kinetic energy of  $\sim 3$  meV (velocities  $< 34\,000$  m/s). These slow electrons are the focus of this Letter. There is also a faint, near uniform signal in the image from electrons outside of the central spot, and these yield a weak, higher energy tail in the  $E_k$  distribution.

The average kinetic energy of the slow electrons is  $< 0.6$  meV, significantly less than the photon bandwidth of 15 meV. As the VUV photon energy is varied, the overall intensity of the images follows the total electron yield spectrum, but the  $E_k$  distributions are nearly identical over the range of photon energies described in this Letter (23–24.5 eV). Fitting the photoelectron angular distributions with the standard expression for anisotropy [12],  $I(\Theta) = 1 + \beta P_2(\cos\Theta)$ , where  $\Theta$  is the angle between the electron velocity and the polarization of the radiation, yields  $\beta = 0$ . Thus the electrons leave the droplet with nearly zero kinetic energy and an isotropic angular distribution.

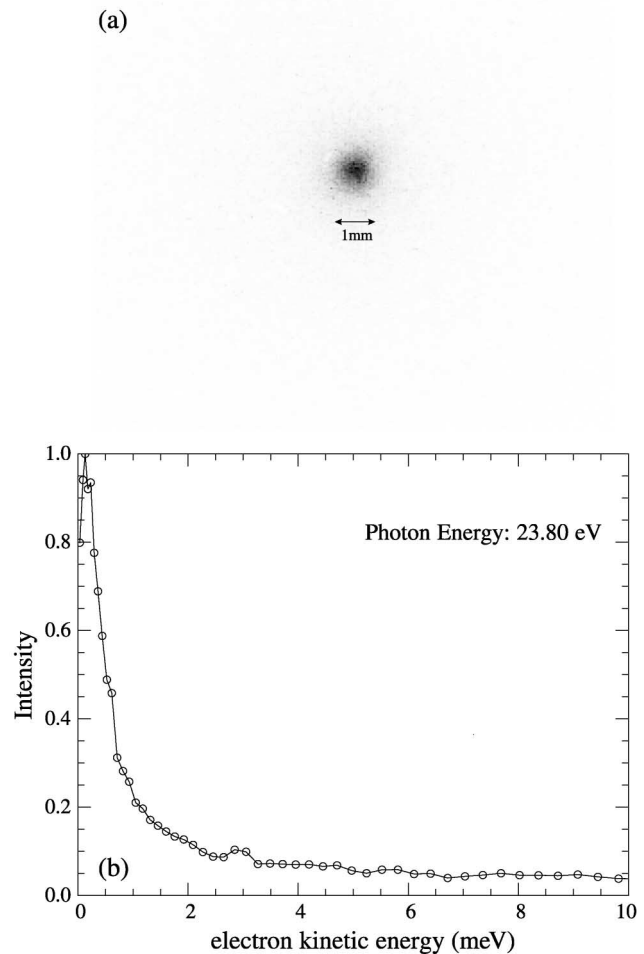


FIG. 3. (a) Raw photoelectron image following 23.8 eV photoexcitation. (b) Photoelectron kinetic energy distribution.

Interpretation of the photoelectron spectra requires an understanding of the electronic excitation process and the subsequent decay channels. Although many-body effects must play a role in the electronic spectroscopy and dynamics of He droplets, processes involving charged and electronically excited  $\text{He}_2$  are important [3,4,6,13] and should be considered as a first step in interpreting our results. The pronounced lowering of the ionization energy of helium droplets compared with atomic helium was attributed by Frochtenicht *et al.* [6] to associative ionization involving formation of  $\text{He}_2^+$  or a larger species within the cluster.  $\text{He}_2^+$  is bound by 2.35 eV relative to  $\text{He} + \text{He}^+$ , and its minimum lies 22.2 eV above that of  $\text{He}_2$ . The threshold for droplet ionization and electron production, 23.0 eV, is 0.8 eV above this value and lies very close to the energy of the  $\text{He}(3p)^1P$  state, the lowest optically allowed atomic state with sufficient energy to form  $\text{He}_2^+$  via associative ionization in collisions with a ground state He atom [14]. In the absence of large perturbing effects, no ionization is expected below Franck-Condon accessible regions of the curve leading to the  $\text{He}(1P3p) + \text{He}$  asymptote, in agreement with our TEY spectrum.

In He droplets, the average He-He nearest neighbor distance is  $\sim 3.6 \text{ \AA}$  [13], while  $R_e = 1.08 \text{ \AA}$  for  $\text{He}_2^+$ , which is comparable to values calculated for the many singlet and triplet excited states of  $\text{He}_2^*$  in the relevant excitation energy range, all of which are Rydberg states correlating to  $\text{He}^*(ns, np, nd \dots) + \text{He}$  [15,16]. Optical excitation thus accesses the asymptotic regions of the potential energy curves, where some of the adiabatic curves are slightly attractive and some are slightly repulsive [16,17]. In the absence of any other effects, one would expect transitions to the repulsive states to lead to  $\text{He}^*$  and transitions to attractive states to lead to highly vibrationally excited  $\text{He}_2^*$ . This species, in turn, can undergo vibrational autoionization or follow other dynamical pathways through its interaction with the surrounding He atoms. For example, von Haeften *et al.* and Northby *et al.* observe partially relaxed  $\text{He}_2^*$  ejected from the cluster [4,18]. This product can result from relaxation of the vibrationally excited  $\text{He}_2^*$  formed by combination on one of the attractive excited states, followed by ejection from the cluster. For states correlating to  $\text{He}^*(3p) + \text{He}$  and higher product states, the initially formed  $\text{He}_2^*$  has enough energy to autoionize to  $\text{He}_2^+ + e^-$ ; this channel would become closed once the  $\text{He}_2^*$  relaxes below the  $\text{He}_2^+$  minimum.

The simplest ionization mechanism would be one in which autoionization to  $\text{He}_2^+$  occurred directly from  $\text{He}_2^*$  before any relaxation, populating one or more of the accessible  $\text{He}_2^+$  vibrational energy levels, with no perturbation from the droplet environment, and with no subsequent electron-droplet interactions. The photoelectron spectrum would then reflect the energy differences between the initial  $\text{He}_2^*$  and the final  $\text{He}_2^+$  states. It is difficult to reconcile this mechanism with the very low

energy photoelectrons observed in our measurements. The  $\text{He}_2^+$  vibrational energy levels are quite widely spaced, with  $\omega_e = 1698.5 \text{ cm}^{-1}$  and  $\omega_e x_e = 35.3 \text{ cm}^{-1}$ , making the near degeneracies between unrelaxed  $\text{He}_2^*$  and  $\text{He}_2^+$  required for very low energy photoelectrons unlikely except at very few excitation energies, whereas we found the photoelectron energy distribution to be nearly independent of excitation energy.

It is possible that electronic excitation and autoionization involves more than two He atoms within the droplet, leading to a vibrationally excited  $\text{He}_n^*$  Rydberg state ( $n < N$ ) that can autoionize via  $\text{He}_n^* \rightarrow \text{He}_n^+ + e^-$ . This process can produce nearly zero kinetic energy electrons, because the much larger density of states in the highly vibrationally excited polyatomic cluster makes it likely that there will always be a near degeneracy between  $\text{He}_n^{**}$  and  $\text{He}_n^+$  vibrational levels. A similar mechanism has been invoked previously; over a large wavelength range, the photoelectron spectrum of  $\text{N}_2\text{O}$  has a small maximum at zero energy that tails off by 20 meV [19]. This feature, which accounts for about 1% of the total photoelectron signal, is attributed to autoionization from vibrationally excited, high Rydberg states of  $\text{N}_2\text{O}$ . However, while this polyatomic autoionization mechanism can explain the presence of low energy electrons over a wide wavelength range, it is less clear that it can be used to explain the dominance of this feature in the He droplet photoelectron spectra.

The observation of very low energy electrons with an isotropic angular distribution and little or no dependence on photon energy is characteristic of a very different ionization mechanism, cluster “thermionic emission,” in which the photoelectron  $E_k$  distribution reflects the cluster temperature [20]. The  $E_k$  distributions in Fig. 3 can fit by  $P(E_k) = A \exp(-E_k/kT)$ , the expected form for thermionic emission from a neutral cluster, with  $T \sim 6 \text{ K}$ . This temperature, which is already close to the original cluster temperature of 0.4 K, represents an upper bound, as the electron signal occurs over very few pixels on the camera. Recent studies [21] of metal cluster anions have shown that photoelectron imaging is extremely sensitive to low energy photoelectrons compared to other photoelectron analysis techniques and is therefore well suited to the observation of thermionic emission.

The situation with He droplets is considerably different than the metal clusters or fullerenes from which thermionic emission has been previously observed [20]. In those systems, electronic excitation above the electron binding energy leads to rapid internal conversion to the ground electronic state, leading a vibrationally hot cluster with a statistical distribution of energy which can “boil off” an electron on a time scale ranging from picoseconds to milliseconds, depending on the size and nature of the cluster. The electron binding energy is lower than or at least comparable to characteristic bond dissociation energies, so that electron emission competes effectively with cluster fragmentation.

In He droplets, the He binding energies are orders of magnitude smaller than the electron binding energy, so it is unlikely that energy randomization subsequent to electronic excitation would lead to electron emission. Nonetheless, our results suggest substantial energy exchange between the photoelectron and the droplet. One mechanism by which this might occur is from autoionization of the  $\text{He}_2^*$  (or  $\text{He}_n^*$ ) Rydberg state injecting an electron into the droplet, which then undergoes collisions with the He atoms prior to leaving the cluster. Under these circumstances, as the outgoing electron slows down, one might expect “bubble” formation, similar to the scenario in bulk liquid helium [22,23] and large clusters ( $> 10^6$  atoms) that support negative charges [24,25]. For example, injection of an electron into liquid He results in formation of a bubble state in  $\sim 10$  ps [23,26]. The electron resides in a cavity, 34 Å in diameter, and has an energy 0.08 eV above the vacuum level. It is predicted that electron bubble states less than 23 Å from the surface are unstable with respect to bubble ejection, for which the barrier is estimated to be as low as 2.5–3.5 meV [27]. The formation and “bursting” of such a bubble in our clusters could be responsible for the low energy photoelectron signal. The higher energy “tail” in Fig. 3 may then result from formation of electrons closer to the surface, allowing for a more direct ejection mechanism.

While there are appealing aspects to the bubble mechanism, some refinement is required because it ignores the Coulomb interaction between the photoelectron and the positive charge created by ionization. This interaction is not present in a negatively charged He droplet. It can be neglected in macroscopic liquid He where there is no limit to the charge separation, but not in our experiments where the droplet diameters are only  $\sim 100$  Å. Thus, one needs to treat the photoexcited droplet as more of an exciton comprising a negatively charged bubble, a positive  $\text{He}_n^+$  core, and the remaining neutral atoms in the droplet. A similar picture was postulated by Buchenau *et al.* [28] to explain the dynamics in He droplets subsequent to electron impact ionization.

One consequence of the Coulomb interaction within the droplet is that the electron will be subject to recapture by the molecular cationic core before it escapes. With very low energy electrons, this should be a rather facile process — one that would explain both the relatively low electron emission yield vs fluorescence (estimated at  $< 1\%$  [6]), and also the observation [4] of emission from triplet states of He and  $\text{He}_2$  which could be ejected from the cluster subsequent to recapture. Triplet states are unlikely to be formed by any optical excitation process. Triplet emission would then begin only when autoionization becomes energetically possible, consistent with the results of von Haefen *et al.* [4]. Finally, the interaction of the Coulomb and helium droplet potentials could result in temporary trapping of the photoelectrons into Rydberg states largely located outside the cluster, as discussed by Golov and Sekatskii [29].

These experiments represent the first step in characterizing the photoelectron spectra of He droplets. Future experiments include measurement of the photoelectron spectra above the He ionization potential, where new ionization channels will be energetically accessible, and a study of cluster size effects on the ionization process. We also plan to undertake studies of He droplets doped with rare gas atoms in order to determine the effect of He solvation on rare gas Rydberg spectroscopy and dynamics.

This work was supported by the Director, Office of Science, Office of Basic Energy Sciences, Chemical Sciences Division of the U.S. Department of Energy under Contract No. DE-AC03-76SF00098.

- 
- [1] J. A. Northby, *J. Chem. Phys.* **115**, 10 065 (2001).
  - [2] J. P. Toennies, A. F. Vilesov, and K. B. Whaley, *Phys. Today* **54**, No. 2, 31 (2001).
  - [3] M. Joppien, R. Karnbach, and T. Möller, *Phys. Rev. Lett.* **71**, 2654 (1993).
  - [4] K. von Haefen *et al.*, *Phys. Rev. Lett.* **78**, 4371 (1997).
  - [5] K. von Haefen *et al.*, *Phys. Rev. Lett.* **88**, 233401 (2002).
  - [6] R. Frochtenicht *et al.*, *J. Chem. Phys.* **104**, 2548 (1996).
  - [7] P. A. Heimann *et al.*, *Rev. Sci. Instrum.* **68**, 1945 (1997).
  - [8] K. Nauta, D. T. Moore, and R. E. Miller, *Faraday Discuss.* **113**, 261 (1999).
  - [9] J. P. Toennies and A. F. Vilesov, *Annu. Rev. Phys. Chem.* **49**, 1 (1998).
  - [10] A. Eppink and D. H. Parker, *Rev. Sci. Instrum.* **68**, 3477 (1997).
  - [11] J. Harms, J. P. Toennies, and F. Dalfovo, *Phys. Rev. B* **58**, 3341 (1998).
  - [12] J. Cooper and R. N. Zare, *J. Chem. Phys.* **48**, 942 (1968).
  - [13] B. E. Callicoatt *et al.*, *J. Chem. Phys.* **109**, 10 195 (1998).
  - [14] T. Fujimoto, Y. Nishimura, and Y. Uetani, *J. Phys. B* **20**, 753 (1987).
  - [15] J. S. Cohen, *Phys. Rev. A* **13**, 99 (1976).
  - [16] S. L. Guberman and W. A. Goddard, *Chem. Phys. Lett.* **14**, 460 (1972).
  - [17] V. Guzielski *et al.*, *Chem. Phys. Lett.* **179**, 243 (1991).
  - [18] J. A. Northby, S. Yurgenson, and C. Kim, *J. Low Temp. Phys.* **101**, 427 (1995).
  - [19] P. M. Guyon, T. Baer, and I. Nenner, *J. Chem. Phys.* **78**, 3665 (1983).
  - [20] J. U. Andersen, E. Bonderup, and K. Hansen, *J. Phys. B* **35**, R1 (2002).
  - [21] B. Baguenard *et al.*, *Phys. Rev. A* **63**, 023204 (2001).
  - [22] J. A. Northby and T. M. Sanders, *Phys. Rev. Lett.* **18**, 1184 (1967).
  - [23] M. Rosenblit and J. Jortner, *Phys. Rev. Lett.* **75**, 4079 (1995).
  - [24] T. Jiang, C. Kim, and J. A. Northby, *Phys. Rev. Lett.* **71**, 700 (1993).
  - [25] M. Farnik *et al.*, *Phys. Rev. Lett.* **81**, 3892 (1998).
  - [26] J. Eloranta and V. A. Apkarian, *J. Chem. Phys.* **117**, 10139 (2002).
  - [27] F. Ancilotto and F. Toigo, *Phys. Rev. B* **50**, 12820 (1994).
  - [28] H. Buchenau, J. P. Toennies, and J. A. Northby, *J. Chem. Phys.* **95**, 8134 (1991).
  - [29] A. Golov and S. Sekatskii, *Z. Phys. D* **27**, 349 (1993).